LINEAR UNIPOLAR PULSE-SHAPING NETWORKS: CURRENT TECHNOLOGY

E. Fairstein*

Abstract

Current usage of linear pulse-shaping filters is reviewed. It is shown that pulse amplifiers with different shaping networks are best compared for spectral resolution and count-rate capability at a shaped-pulse width measured at a specific fraction of peak height, preferably 50% ($t_{1/2}$). With this normalization, it is shown that the best tradeoff between noise and resolving time is obtained with the quasi-triangular waveform, the worst with the cusp.

Noise, resolving time, and ballistic deficit are compared through graphs and tables for the cusp, true Gaussian, true triangle, CR-$(RC)^n$, sine^n, and quasi-triangular shapes for normalizations at t_p, $t_{1/2}$, and $t_{.01}$. Rules are given for estimating the effect of pulse shape on noise performance.

A. List of Symbols

Specialized symbols used frequently in this report are listed below; standard symbols for electrical and physical quantities are not. Unless otherwise specified, units are in kelvins, amperes, coulombs, farads, ohms, seconds, and volts. Squared quantities enclosed in carets, such as $\langle \zeta^2 \rangle$, refer to noise signals in mean-squared units (variance). Unsquared quantities, such as $\langle \zeta \rangle$, denote root-mean-squared values. Subscripts i, p, and f used in connection with noise symbols denote impulse (delta), step, and flicker ($1/f$) noise respectively.

a	Parameter for changing the width of a pulse. See x.
b	Parameter for translating a pulse along the time axis. See x.
BD	Ballistic deficit.
$\langle C_c \rangle$	Noise-equivalent input capacitance of a preamplifier ('cold' input capacitance).
CR	High-pass filter (differentiator).
e_o	Electronic charge, 1.602 x 10^{-19} C.
$F(t)$	Function of time. Also, network transfer function in the time domain.
$F(t_o)$	Peak amplitude of a pulse, also $F(x_o)$.
$F(x)$	Function of x. Also, time-normalized network transfer function. See x.
$F(x_o)$	See $F(t_o)$. The quantities are numerically identical.
G_M	Transconductance.
$G(\omega)$	Network transfer function in the frequency domain.
LE	Leading edge of a pulse.
LE_y	Point in time measured on the leading edge of a pulse at the fraction y of its peak height.
ms	Mean square.
n	Number of low-pass sections in a filter ne work, as in CR-$(RC)^n$.
NSR	Noise to signal ratio.
ppk	Parts per thousand.
R_p	Noise-equivalent parallel (shunt) resistance.
R_s	Noise-equivalent series resistance.
RC	Low-pass filter section (integrator).
rms	Root mean square.
SNR	Signal to noise ratio.
T	Duration of the rising portion of a ramp th terminates in a unit-height signal. Als charge collection time in a detector.
T_ϵ	Temperature.
TE	Trailing edge of a pulse.
TE_y	Point in time measured on the trailing edge a pulse at the fraction y of its peak height.
t_p	Peaking time (the time interval between LE and the peak of a pulse. See LE_y).
t_w	Width of a rectangular pulse equal in amplitu and area to the one under consideration.
t_y	Width of a pulse measured at the fraction y of its peak height.
τ	Time constant (in seconds unless otherwi specified).
x	$at + b$, pulse shape altered in width by the pa ameter a and translated along the time a by the parameter b.
y	Fraction of peak height at which a time mark established.
$\langle \xi^2 \rangle$	Numerical portion of mean-squared noi index $\langle \zeta^2 \rangle$. Values appear in Table 2.
$\langle \zeta^2 \rangle$	Mean-squared noise index as determined l the shaping network, less factor due to noi generator.

B. Introduction

The purpose of this report is to explore the concept pulse-width normalization and its application to the me urement and computation of spectral resolution, amplifi noise, resolving time, and ballistic deficit. In the proc the preceding items will be reviewed, showing how t concept of normalization may lead to new perspectives.

C. Spectrometer Tests

Usually, it is assumed that amplifiers with differe linear pulse shaping networks exhibit easily-distinguisha performance differences. This seems to be borne out the information displayed in Fig. 1, which is a set of cur

*c/o Tennelec, Box 2560, Oak Ridge, TN 37831

of spectral resolution vs the 'Shaping Time' indications on the front panels of several commercially available amplifiers. Three different shaping networks are represented. The tests were made at 2 and 62 kilocounts per sec (kCPS). The resolution is essentially the same for all of the amplifiers, but the minima at each of the two counting rates occur at different dial settings. Two conclusions may be drawn: if only one measurement were made at, say, 3μs or 6μs, at least one of the units in the group would suffer from a resolution comparison, or, if the minima were sought for all of the amplifiers, the user still might conclude that one with a minimum at a lower dial setting would yield superior count-rate performance. Neither conclusion would be justified.

In Fig. 2, the same curves are shown, but this time plotted against $t_{1/2}$ (width of the shaped pulse at 50% of its peak height*). Clearly, at the minima of the 2 kCPS curves, all of the amplifiers now show equivalent performance. The same is true at the 62 kCPS minima, but at the ends of the curves, the departures that do appear are genuinely attributable to the differences of the various shaping networks and to other aspects of amplifier design.

Fig. 2 illustrates what can be described as 'pulse-width normalization', a process in which pulse shapes having different mathematical descriptions are compared in width at a fraction y of their peak heights. This normalization simplifies the performance comparisons referred to earlier. Several other normalizations are possible (Figs. 3 and 4). Before they are investigated, shaping networks of current interest will be examined.

In the descriptions to follow it is often awkward to distinguish the pulse shape from the network that produces it, and no particular effort will be made to do so. The reader should understand that referring to one implies the other.

D. Shaping-Network Configurations, General Considerations

Equivalent terms for a shaping network are noise filter, pulse shaper, filter network, or just filter.

What counts for performance is the shape that is generated as viewed on an oscilloscope, not the filter configuration or its mathematical description per se.

Six pulse shapes are studied here, and where appropriate, the networks that generate them: the cusp, true Gaussian, true triangle, quasi-triangle, CR-$(RC)^n$ and sine^n.

The cusp is not physically realizable, but represents an upper limit to the attainable SNR in linear filters [2]. The true Gaussian is not realizable either, but represents the asymptotic limit of quasi-Gaussian waveforms. The true triangle is realizable, but not in a cost-effective way. Its shape is the asymptotic limit of a quasi-triangular waveform. Of the realizable waveforms the quasi-triangular and sine^n are the current choices among manufacturers of amplifiers.

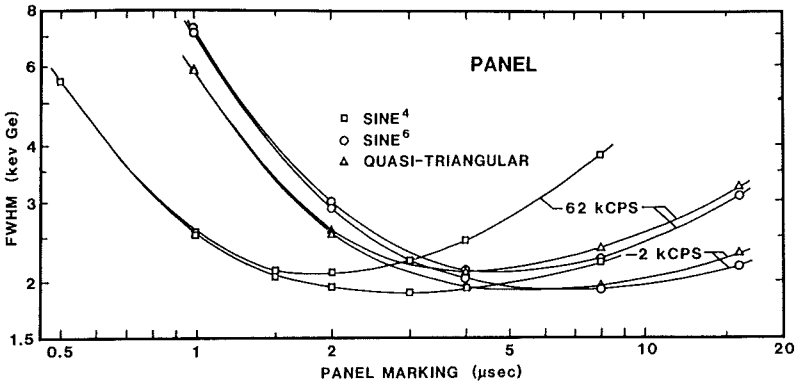

Fig. 1. Energy resolution tests of three different shaping networks and three different amplifiers. (Two of the amplifiers were so nearly alike that the data from only one is displayed.) The 1.33 MeV γ-ray from ^{60}Co and a high-purity germanium detector produced the signals. The shaping times were those indicated by the dials on the front panels. Results are shown for 2 and 62 kCPS.

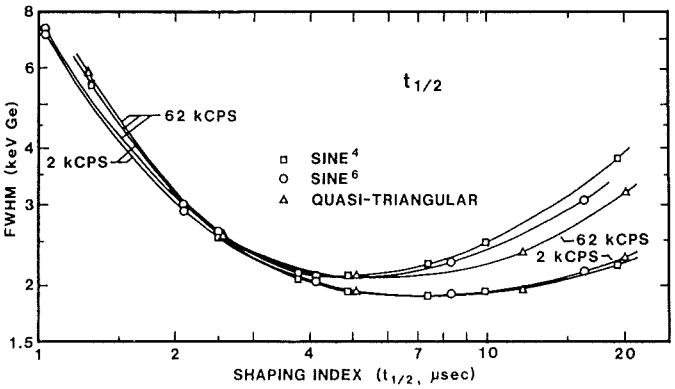

Fig. 2. Same as Fig. 1, but the Shaping Index $t_{1/2}$ is used instead of the amplifiers' dial markings for the shaping-time axis. The Shaping Index is the measured pulse width at 50% of peak height.

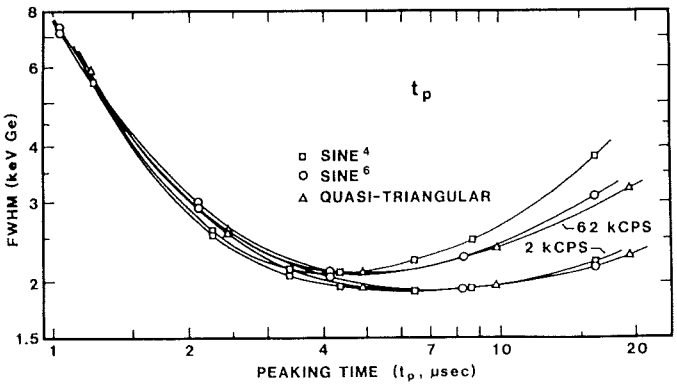

Fig. 3. Same as preceding figures, but with peaking time t_p as the scale for the shaping-time axis. The peaking time is measured from 1% of peak height on the leading edge of the pulse to the center of the peak.

*What prompted the study reported here is a remark made several years ago by G. L. Miller (at a meeting of the IEEE Nuclear Instruments and Detectors Committee) that the SNR obtained with various shaping networks depended more on the width of the shaped pulse than on any other parameter. At that meeting, we were working on an update of the standard for amplifier testing, IEEE Std 301. It was particularly appropriate to pursue the suggestion. In the updated standard [1], $t_{1/2}$ was adopted as the descriptor of shaped pulse width and was given the name 'Shaping Index' to which the term refers exclusively.

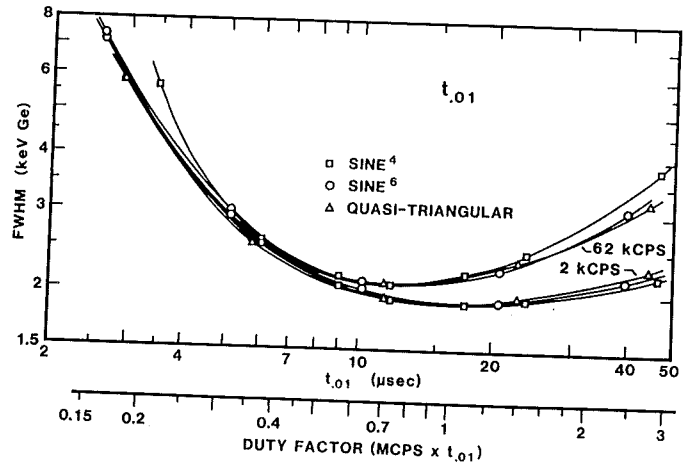

Fig. 4. Same as preceding figures, but with $t_{.01}$ (width at 1% of peak height) as the scale for the shaping-time axis. This figure includes a scale for the duty factor, which is defined here as the ratio of shaped-pulse width (at the 1% level) to the mean spacing between events in the detector. The duty factor can exceed 1.0 because with randomly-arriving events, shaped pulses can overlap. The clear regions between those groups of overlapped pulses average to the reciprocal of the duty factor.

The symbol usually used in equations that describe pulse shapes is t/τ, where τ is a network time constant. For simplicity in this section of the report, unit τ is assumed.

The following three 'ideal' pulse shapes are characterized by the equations accompanying them. In each case, the peak amplitude is of unit height and occurs at $t = 0$. The parenthetical letter following the name of the waveform identifies it in the graphical presentations.

Cusp (C) $\quad F(t) = e^{-|t|}$ (1)

True Gaussian (G) $\quad F(t) = exp(-t^2)$ (2)

True Triangle (Δ) $\quad F(t_-) = (1 + t),\ -1 \le t \le 0$
$\quad F(t_+) = (1 - t),\ 0 \le t \le 1$ (3)

The next three filters are the realizable ones.

CR-(RC)^n (E) $\quad F(t) = [t^n/n!]e^{-t}$ (4)

This filter contains one high-pass section followed by n low-pass sections, all with the same time constant. The configuration is known as a quasi-Gaussian filter because the response to a step input approximates that of the Gauss error curve $exp(-t^2/2\sigma^2)$, or $exp(-t^2)$ if $2\sigma^2 = 1$. The name is not as fitting as it could be because Eq. 4 is that of a Poisson distribution. (If the connection between the waveform and the distribution is other than accidental, the reason is not obvious to this writer.)

The *CR-(RC)^n* filter is not used in modern amplifiers because better perfomance can be obtained with the same number of filter sections but with dissimilar time constants. However, because of its mathematical simplicity, the more primitive network is of interest for modelling. In a variation not addressed here but used in some amplifiers, the integrators contain complex poles, all with the same time constant. The performance is intermediate between that of the *CR-(RC)^n* and sine^n networks.

Sine^n (S) $\quad F(t) = K_s\, e^{-3t} \sin^n t$

The sine^n network [3] was so named because of preceding descriptive equation. The constant K_s is a fa that depends on the circuit configuration. The waveform that of a highly damped sine wave raised to the nth po where n is the number of low-pass sections contained the network. The damping is so great that only the fi half cycle is significant, with the next one down in am tude by a factor of $\approx 10^{-4}$. If n is even, all successive h cycles (satellite pulses) have the same polarity as the fi Mathematically, the network exhibits a real pole at t = and n complex pole pairs at $\pm 2jt$, $\pm 4jt$, $\pm 6jt$ . . . on a li passing through t = -3.

Quasi-triangular (QT)

$$F(t) = e^{-3t}(7.64 \sin^2 t + 2.53 \sin^4 t + 37.74 \sin^6 t) \quad (6$$

The waveform [4], despite its rounded top, is so named because of the association of its straight sides with those of a triangle. The shape is obtained by summing fractions of the outputs from the several integrators that comprise the basic network, which can be *CR-(RC)^n*, sine^n, or other. With this summing, the signals from the earlier integrator sections reduce the inherent delay in the start-up of the output pulse without causing much change in the position of the peak or in the already nearly-linear trailing edge. This filling-out of the lower part of the leading edge produces the nearly straight-line rise and improves the overall symmetry.

In this report the originating network for the QT filter is the sine^6 network. The response to a step-function input is given by Eq. 6. With the multipliers shown, t_o (defined in Fig. 5) = 1.014437 and $F(t_o)$ = 1.00010. Within rather narrow limits, the ratios of the constants are subject to the discretion of the circuit designer. The constants chosen here were determined largely by trial and error to optimize the *SNR* and the linearity of the leading edge while simultaneously producing values for t_o and $F(t_o)$ near unity.

E. Waveform Terminology

The shape of the waveform as displayed on an oscilloscope is shown in Fig. 5. The parameters defined in the figure, and others that can be inferred from it—$t_{0.1}$, $t_{.001}$, etc.—are used throughout this report. The symbol x may be substituted for t if the waveform has been altered in width or translated along the time axis.

In the figure, the pulse occupies exactly five major divisions vertically. To accurately measure $t_{.01}$, the oscilloscope sensitivity should be increased x10. This causes the skirts of the pulse to move upscale as shown by the line segments so labelled. The corresponding scale is shown to the left of the main one. The symbol t_o refers to the time interval between the start of the generator signal and the

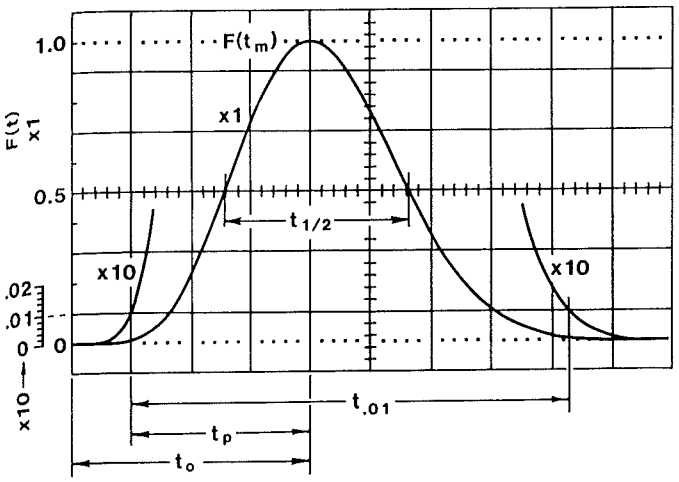

Fig. 5. Oscilloscope display of a typical shaped pulse that is vertically centered on the the CRT graticule to aid in the measurement of key parameters. The oscilloscope and amplifier must be dc coupled.

peak of the pulse under observation. Note that t_o, the mathematical peaking time, is different from t_p, which is measured from the 1% level on the leading edge.

F. Time-Normalized Pulse Shapes

In the usual way of presenting pulse shapes, the abscissa is in units of at, where $a = 1$, while the ordinate is in units of amplitude normalized to unit peak height. Such a presentation is shown in Fig. 6 for the CR-$(RC)^n$ and sine^n networks. The sine^n family is contained between the S2 and S16 waveforms. They crowd together because of the single real pole mentioned earlier. The multiple real poles of the CR-$(RC)^n$ waveforms cause them to spread along the time scale; t_o (not t_p) is numerically equal to n. In the format shown here, noise performance, ballistic deficit, and resolving time can be determined for any one of the waveforms, but it is not at all clear how to compare them for peformance.

In Figs. 7, 8, and 9, the normalizations are to unit t_p, $t_{1/2}$, or $t_{.01}$, with the waveforms shifted along the time axis so that all pass through the chosen normalization points.

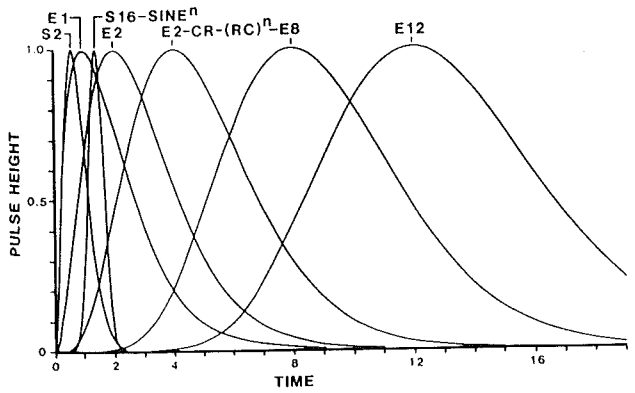

Fig. 6. Sine^n (S) and quasi-Gaussian (E) waveforms normalized to unit amplitude, but not to units of time. The numerals refer to the number of integrating sections in the networks giving rise to the waveforms.

Presented this way it is relatively easy to compare chosen characteristics:

In the t_p normalization resolving times and asymmetry at the 1% level are accentuated (asymmetry is detrimental to impulse-noise performance).

In the $t_{.01}$ normalization the resolving time is fixed, causing the indication of asymmetry to appear as peak shift along the time axis.

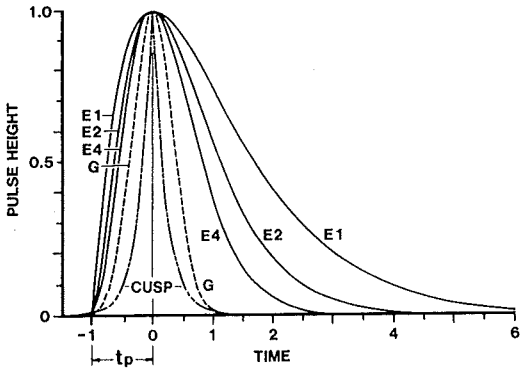

Fig. 7. Pulse shapes normalized to $t_p = 1$ and with $F(t_o)$ centered on $t = 0$. Symbol G refers to true Gaussian.

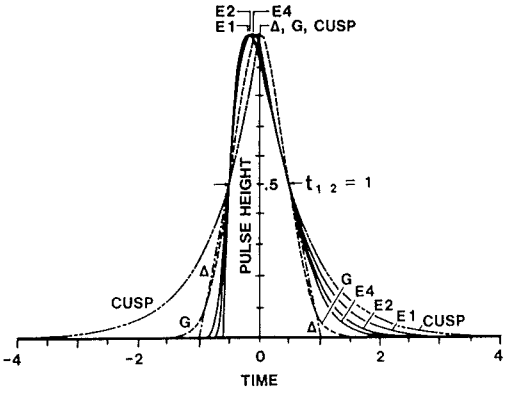

Fig. 8. Same as Fig. 7, but normalized to $t_{1/2} = 1$. The triangle (Δ) was added to the ensemble.

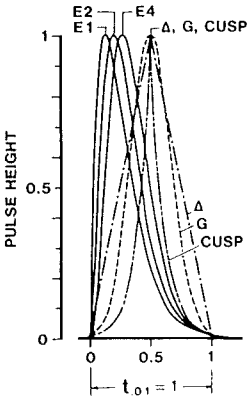

Fig. 9. Same as Fig. 7, but normalized to $t_{.01}$. The 1% point on the leading edge is taken as $t = 0$.

In the $t_{1/2}$ normalization, differences between curves are minimized, resulting in nearly constant step noise for the different curves, as will be shown later. Also, the curvatures at the tops of the waveforms are minimized, resulting in nearly constant ballistic deficit (BD).

In Fig. 10 all of the waveforms are combined in a semi-

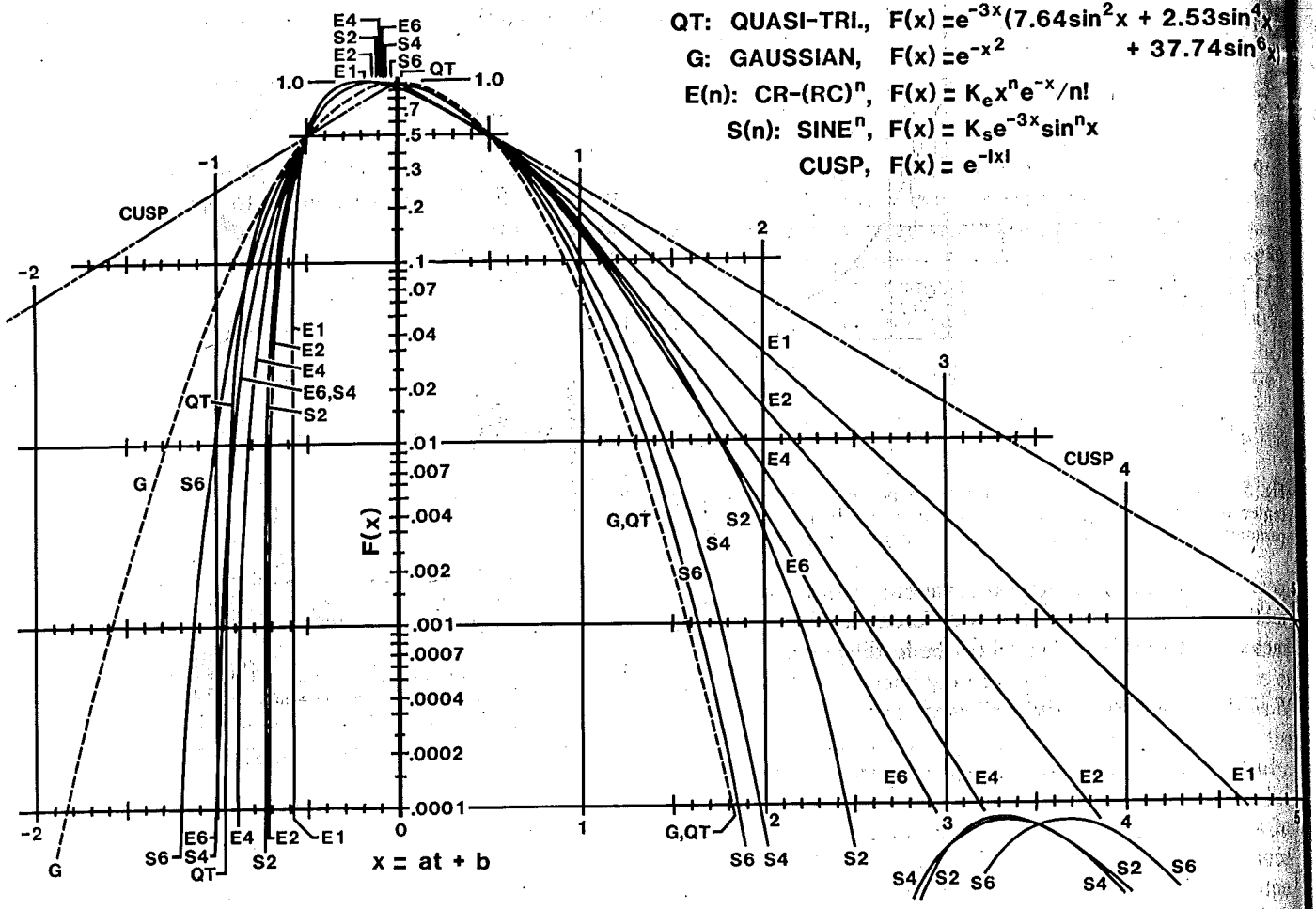

Fig. 10. Pulse shapes normalized to $t_{1/2}$ and plotted to a semilog scale.

log plot normalized to $t_{1/2}$, giving both a panoramic view of resolving time (down to 0.01% of peak height) and of the degree of symmetry for the various pulse shapes. In this plot, the second-order artifacts of the sine^n waveforms appear in the lower right-hand corner, illustrating the earlier statement about the amplitude and polarity of the satellites. Also, the poor resolving time of the cusp—which has straight lines for leading and trailing edges in a semilog plot—is made clearly visible.

To determine the scale factor a and the translation parameter b for each of the normalized waveforms, the times of the leading- and trailing-edges (LE and TE) at the normalization level y must be determined for each of the originating waveforms: those for which $a = 1$ and $b = 0$. Except for the cusp, true triangle, and true Gaussian, there are no explicit formulas for doing this; they must be found by solving the equation $[F(t)/F(t_o)] - y = 0$ by a numerical root-finding process, where $F(t)/F(t_o)$ is the waveform normalized to unit amplitude and y is the desired fractional amplitude level: 0.5, 0.01, etc. Then:

$$a = TE - LE \tag{7}$$

If the waveforms are to be centered at $t = 0$, as they are in Fig. 10, then:

$$b = 0.5\,(TE + LE) \tag{8}$$

The terms TE, LE, and a are given in Table 2 along with other information. Parameter b can be computed as needed using Eq. 8.

The study now moves on to the possible normalization factors and how they affect other parameters of interest.

G. Choice of Normalization Factor based on Waveform Measurement

Although different normalizations may be desirable to emphasize particular features of a filter network, a single standard is preferred, both for simplicity and for the practical need of labelling the shaping-time dial on an amplifier —the units should be recognizable by all users of the equipment. In choosing a standard, four criteria come to mind: (1) ease and accuracy of measurement, (2) how t_y relates to noise filtering, (3) to resolving time, and (4) to ballistic deficit. Among the possible choices for a standard are t_w, t_p, $t_{1/2}$, $t_{0.1}$, $t_{.01}$, and $t_{.001}$.

H. Choice of t_y Based on Ease of Measurement

Width at t_w. To obtain this parameter [5], the area of the

pulse must be determined, either by computing it from the equation that describes it or by measuring it from an oscilloscope display. Both methods are cumbersome. As for the usefulness of t_w, it can be shown that it does not bear a simple relationship to noise or to ballistic deficit, nor is it helpful for its historical purpose of computing baseline shift vs counting rate in an amplifier containing a baseline restorer (*BLR*), a subsystem [6], [7] that is part of all modern spectrometer-grade amplifiers. In short, t_w is neither easily measured nor useful, and will receive no further attention here.

Peaking Time (t_p). This parameter has two drawbacks regarding measurement accuracy: the instant of the peak is poorly defined because it occurs where the slope of the waveform is zero, and to determine the 1% point on the leading edge, the extra step of increasing the oscilloscope sensitivity is necessary (see Fig. 5).

Shaping Index ($t_{1/2}$). Of the possible normalizations considered here, this one can be measured with the fewest number of steps and with the greatest accuracy: no change in oscilloscope sensitivity is necessary after the original calibration (see Fig. 5), and the measuring points fall where the slope of the waveform is high.

Width at the 1% Level ($t_{.01}$). This parameter has the merit of approximating the amplifier resolving time, but if that's the criterion, why $t_{.01}$? Why not $t_{0.1}$, or $t_{.001}$? The answer lies with the operating characteristics of the *BLR*.

A *BLR* is a circuit that immediately after a pulse restores the baseline to where it was just prior to it. The effective resolving time is fixed by the *BLR*: when it loses control at high counting rates, the spectral resolution rapidly worsens, particularly at FW.1M. The *BLR* retains control as long as it can reset in the gaps between pulses or between groups of overlapping pulses. However, as the counting rate increases, a point is reached where the gaps are no longer frequent enough or long enough for resetting to occur. This condition contributes to the loss in resolution at the longer shaping times in the 62 kc/s curves of Figs. 2-4.

The *BLR* is most effective when its operating threshold is just above the peak noise. If the threshold is set at three times the *rms* noise level, only 0.1% of the noise pulses will exceed it, but because of possible drift, it is safer to set it at ≈six times. It is necessary to know what that level is, expressed as a fraction of the peak pulse height:

Suppose that a spectrometer is set up to measure 1-Mev γ-rays with a germanium detector, that the component of FWHM due to noise is 1 keV (0.001 MeV), that the amplifier has a dynamic range of 10V, and that the gain is set to produce 7V pulses. It follows that the threshold will be at [(7V/10V) x (0.001 MeV)/(1 MeV) x 6/2.35] = 0.18% of rated maximum output (the factors 6 and 2.35 refer to the BLR threshold and the conversion constant of *rms* to FWHM). Based on that, the choice of $t_{0.1}$ is inappropriate, but it is reasonable to choose either $t_{.001}$ or $t_{.01}$. However, $t_{.001}$ is subject to large measurement error, and even $t_{.01}$ is vulnerable, as shown by the varying recovery times of the waveforms in Fig. 11, which were obtained with several combinations of *BLR* and *P/Z* (pole/zero) adjustments in a modern amplifier set at its longest shaping time. In the figure, the *BLR* settings are those which might normally be used, but the *P/Z* settings are misadjustments that easily could occur in practice. The point is that by deliberate or accidental misadjustment of amplifier controls, the pulse width at the 1% level is poorly defined, whereas those same (mis)adjustments do not noticeably affect the pulse width at the 50% level.

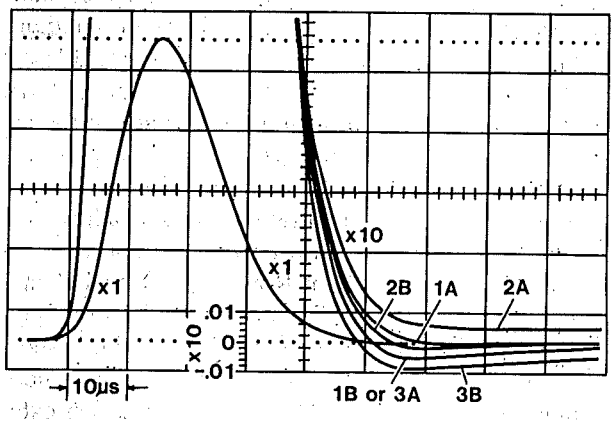

Fig. 11. Pulse recovery to the 1% level with several settings of the BLR and P/Z controls. The waveform occupying 5 major divisions is at a relative sensitivity setting of x1. The vertically-expanded set is at x10 sensitivity. The conditions are indicated by a combination of letters and numbers. Letters: (A) BLR OUT; (B) BLR IN, high count-rate setting. Numbers: (1) P/Z correctly set; (2) P/Z 0.5% overcompensated; (3) P/Z 0.5% undercompensated.

Recapitulation. Of the likely pulse-width normalizations, only t_p, $t_{1/2}$, and $t_{.01}$ merit serious consideration. Of the three, $t_{1/2}$ is the easiest to measure and with least ambiguity.

1. Ballistic Deficit

Ballistic deficit is the loss in pulse height that occurs at the output of a shaping network when a step-function driving signal has greater than zero risetime. The loss is accompanied by a delay in the peaking time. The delay can be used as a measure of the *BD* in the implementation of compensating schemes.

The rising portion of the driving signal can have various shapes, but in this report, it is assumed to be a linear ramp of duration T, causing a delay in the shaped-pulse peaking time t_o of $\approx T/2$. The shifted peak will appear at time t_m. If the pulse is normalized by the factor a, then t_o becomes $x_o = at_o$, and t_m becomes $x_m = at_o$.

In a spectrometer the detector constitutes the signal source; T is the charge collection time. With shaping networks that have a continuous derivative at the peak, the loss of pulse height that occurs is proportional to T^2, which varies randomly from pulse to pulse. The loss in amplitude is not important, but the variation is, because it causes spectral-line broadening. The effect in the CR-$(RC)^1$ network was investigated by Gillespie [5], then by Baldinger and Franzen [8]. The study was extended to the CR-$(RC)^n$ network and to one with complex poles by Loo, Goulding, and Gao [9]. A method of compensating the effect was

described by Goulding and Landis [10].

J. Choice of Normalization based on Ballistic Deficit Considerations

Loo, Goulding, and Gao (LGG) showed that if the width of a shaped pulse is measured at the 90% level, the *BD* can be determined for an *n*th-order quasi-Gaussian network from a table published in their paper. If the pulse widths are normalized instead to $t_{0.9}$, the determination can be simplified. As can be seen from Row Y in Table 2, the *BD* is virtually invariant with pulse shape for that condition, confirming LGG's finding, but also adding to the argument in favor of normalization. However, $t_{0.9}$ is not as easily measured on an oscilloscope as $t_{1/2}$.

With $t_{1/2}$ as the normalization, the dependence of *BD* on network complexity is shown in Fig. 11 and in Row DD of Table 2. Examination of Rows V, DD, and II in Table 2 shows that among t_p, $t_{1/2}$, and $t_{.01}$, $t_{1/2}$ is the best choice.

With the *CR*-$(RC)^n$ network the *BD* diminishes monotonically as n increases, but with the sine^n network, a minimum occurs at $n = 4$. This configuration exhibits the lowest *BD* (by 11%) of any of the networks, including the true Gaussian and quasi-triangle. It appears that the variation is small enough to make *BD* a poor criterion for choosing one linear network configuration over another.

In every instance the peak shift is very nearly 50% of the ramp time T (Row EE in Table 2); for pulses with perfect symmetry, the shift is exactly 50%. Not surprisingly the cusp and true triangle, which have discontinuous derivatives at their peaks, exhibit very high *BD*'s, with the cusp being the worst. Also, the *BD* for such pulses varies linearly as T/t_y rather than as the square.

The figures in Table 2 are based on a charge-collection time of $T = 0.1$ time units (10% of t_y) when the rate of rise is constant. The rationale for the choice is as follows:

In the larger germanium detectors, collection times of 0.25μs are not unusual [11]. During a pulse, the rate of rise can vary ≈x2 from start to finish, depending upon where in the detector the ionization occurs. Although T may be as large as 0.25μs, the variation is unlikely to be much greater than 0.1μs, hence the choice of 0.1.

K. Computations of Ballistic Deficit for $t_{1/2} = 1$

In this section the earlier work [5], [8]- [10] is extended to the networks covered in this report.

Straightforward circuit analysis using Laplace transforms or convolution [9], [12] gives exact values for *BD*. For a network of order n, both methods give rise to two series of n terms each, one in $F(t)$ and the other in $F(t - T)$. The *BD* is the difference between the two summations. Separately, they do not vary much with n, but the difference diminishes as the *BD* decreases, leading to large errors in those differences. Also, unless the precise value of the peaking time of the delayed pulse is used in the computation, the error is compounded. With pocket calculators, the method falls apart in the vicinity of *BD* = 0.1%. However, below 1%, the *BD* is closely proportional to T^2, permitting accurate extrapolation. Regardless of attainable precision, lengthy computation is required.

A much simpler method due to Baldinger and Franzen [8] has fewer terms, and small differences between large numbers do not occur. The method depends on a Taylor series expansion about the peaking time of the pulse *before* it is shifted by *BD*, which in itself is a major simplification because it avoids the need to determine accurately the location of the shifted peak. The series converges rapidly: using only the first term, the resulting error is high by ≈1% for a *BD* of 1%, or by ≈10% for a *BD* of 10% (10% becomes 11%). Adding a second term reduces the error by the square (1% becomes 0.01%), usually overshooting on the low side. A *BD* of 10% probably exceeds the correction capability of any practical compensating scheme, making it unnecessary to consider greater *BD*'s or the more difficult method of computation discussed earlier. Nevertheless, both methods are covered here for comparison.

The Baldinger-Franzen approximation, with the original second-term factor 1.1 changed to 0.9, is shown in Eq. (9). (The factor 0.9, arrived at empirically, gives higher accuracy than the original.)

$$BD = M^2 (1 - 0.9M^2) \tag{9}$$

$$\text{where } M^2 = \frac{(aT)^2}{24} \frac{F''(t_o)}{F(t_o)},$$

$F''(t_o)$ = second derivative of $F(t)$ at $t = t_o$,

$F(t_o)$ = $F(t)$ at $t = t_o$.

In Table 1, the following quantities are listed: the curvature $F''(t_o)/F(t_o)$, the peak position of the undisturbed pulse, and the peak position shifted by *BD*. Also given are the values of a for which $n = 6$ and $t_{1/2} = 1$ in the *CR*-$(RC)^n$ and Sine^n functions, and a for $t_{1/2} = 1$ for the remaining functions (n does not apply). Additional formulas are given under the pertinent network headings, and numerical examples for a ramp time of $T = 0.7\,t_{1/2}$ are giv-

Table 1

Curvature and peak position for the CR-(RC)^n (E), Sine^n (S), Quasi-Triangular (Q-T), and True-Gaussian (G) networks, normalized to $t_{1/2} = 1$ and $n = 6$. The curvature is proportional to $F''(t_o)/F(t_m)$. The term x_m is the position of the time-normalized peak, shifted by BD from its original position at x_o. Note that initial peak height $F(x_o) = F(t_o)$.

Network	$\frac{F''(t_o)}{F(t_o)}$	x_o	x_m	a for $t_{1/2} = 1$, n = 6 (for E & S)
E	$1/n$	n/a	$T(1 - e^{-aT/n})$	5.8052
S	$n + \frac{9}{n}$	$\frac{\tan^{-1}(n/3)}{a}$	$\tan^{-1} \frac{\sin aT}{(\cos aT) - e^{-3aT/n}}$	0.8477
Q-T	-5.5023	$1.014437/a$	No explicit expression	1.0383
G	-2	0	T/2	1.6651

en. This T causes a BD of ≈10% in pulses having continuous derivatives at their peaks.

In Table 2, T = 0.1 causes BD's of ≈0.25%. Based on a T^2 relationship, the BD for T = 0.7 should be 0.25% x $(7)^2$ = 12.25%, but as can be seen, the actual BD is somewhat lower. For the cusp, the BD at T = 0.1 is ≈3.4%. At T = 0.7, the BD should be 3.4 x 7 = 24% based on a linear relationship; the actual BD is ≈20%.

CR-(RC)^n Network. The exact formula for the BD of this network is:

$$BD = 1 - \frac{F(x_m)}{F(x_o)} \qquad (10)$$

$$= \frac{n!e^n}{n^n} \frac{exp(-x_m)}{aT} \sum_{k=0}^{n} \left[\frac{x_m^k}{k!} - \frac{e^{aT}}{k!}(x_m - aT)^k\right]$$

where $1/F(x_o) = n!e^n/n^n$, the inverse of the peak height of the output signal in the absence of BD. The other terms are given in Table 1.

For n = 6
T = 0.7 (70% of $t_{1/2}$ = 1)

Exact BD = -10.34%
1st-Order Approx. = -11.47% (Baldinger Franzen)
2nd-Order Approx. = -10.28% (Baldinger Franzen)
x_o = 1.0336
x_m = 1.4227
$x_m - x_o$ = 0.3891 = 0.556aT

Sine^n Network. The exact formula for the BD is given in Eq. 11. As in the case of the *CR-(RC)^n* network, the generic form of Eq. 10 also applies here.

$$BD = \frac{n!exp(-3x_m)}{aTK} \sum_{\substack{k=0,\\ k\ even}}^{n} \frac{[3\sin^k x_m - k\sin^{(k-1)}x_m \cos x_m] - e^{3aT} F(x_m - aT)}{\prod_{\substack{\omega = k\\ \omega\ even}}^{n} (9 + \omega^2)} \qquad (11)$$

The term $F(x_m - aT)$ is a repeat of the preceding bracketed term, but with $(x_m - aT)$ substituted for x_m where it appears in the sine and cosine terms. The term x_m is given in Table 2, and K is the the peak height of the output pulse in the absence of BD. That signal is:

$$F(t_o) = exp(-3t_o)\sin^n t_o, \qquad (12)$$

where $t_o = \tan^{-1}(n/3)$

For n = 6
T = 0.7 (70% of $t_{1/2}$ = 1)

Exact BD = -10.067%
1st-Order Approx. = -11.005% (Baldinger Franzen)
2nd-Order Approx. = -9.915% (Baldinger Franzen)
x_o = 1.3059
x_m = 1.6733
$x_m - x_o$ = 0.3674 = 0.525aT

The sine^6 network exhibits a slightly lower BD than the *CR-(RC)^6* filter.

Quasi-Triangular Network. The exact formula for the BD of the quasi-triangular network is more complicated than the preceding ones because the waveform is the sum of three terms in sine^n. Furthermore, there are no closed-form equations for the peak heights of the pulses—they must be determined from $F'(t) = 0$ or $F'(x) = 0$ by a numerical root-finding procedure. The exact equation for the BD is given below. Because of its length, it is split into groups of terms.

$$BD = [1 - \frac{F(x_m)}{F(x_o)}] \qquad (13)$$

where

$$F(x_o) = exp(-3x_o)[Xy^2 + Yy^4 + Zy^6]$$

$$Fx_m = \frac{n!exp(-3x_m)}{aTK}\{[3F1(y) + yzF2(y)] - e^{3aT}[F(y,z - aT)]\}$$

$y = \sin x_m$
$z = \cos x_m$
$F1(y) = Zy^6 + Yy^4 + Xy^2 + 2X/9$
$F2(y) = 6Zy^4 + 4Yy^2 + 2X$
$F(y, z - aT)$ = all preceding x_m terms in y and z replaced by $(x_m - aT)$.

$$X = \frac{25A + 12B + 8C}{13 \times 25} = 1.6101$$

$$Y = \frac{3B + 2C}{75} = 1.1076$$

$$Z = \frac{C}{45} = 0.8387$$

A = 7.64
B = 2.53
C = 37.74
K = 1.0001

Constants A, B, and C are those appearing in front of the sine^2, sine^4, and sine^6 terms, respectively, in Eq. 6.

The quasi-triangular network exhibits a slightly higher BD than either the *CR-(RC)^6* or sine^6 networks. This is to be expected because for the same $t_{1/2}$ the linear rise of the leading edge of the quasi-triangular pulse, compared with the S-shaped rise of the *CR-(RC)^6* and sine^6 signals, forces a sharper peak at the top.

True Gaussian, $F(x) = exp(-x^2)$. Only the Baldinger-

Franzen approximation is given here.

$$\begin{aligned} \text{For } T &= 0.7 \text{ (70\% of } t_{1/2} = 1) \\ a &= 1 \end{aligned}$$

$$\begin{aligned} \text{1st-Order Approx.} &= -11.32\% \text{ (Baldinger Franzen)} \\ \text{2nd-Order Approx.} &= -10.16\% \text{ (Baldinger Franzen)} \\ x_o &= 0 \\ x_m &= 0.3500 \\ x_m - x_o &= 0.3500 = 0.5aT \end{aligned}$$

Gillespie's [6] criterion for a maximum of 0.5% *BD* called for the time constant of the *CR*-$(RC)^1$ filter to be greater than three times the charge collection time in the detector. In the preceding examples, the criterion should be seven times because of the normalization to $t_{1/2}$. Furthermore, the criterion holds regardless of the network complexity.

The criterion does not apply to the cusp and the true triangle because of the discontinuous derivatives at their peaks. Also, the Baldinger-Franzen method does not apply, nor is it necessary because the exact formulations of *BD* are simple.

Cusp, F(x) = $e^{-|x|}$. As formulated here, the cusp has unit height, reducing $F(x_m)/F(x_o)$ to just $F(x_m)$.

$$\begin{aligned} \text{For } T &= 0.7 \text{ (70\% of } t_{1/2} = 1), \\ a &= 2(\ln 2) = 1.3863 \end{aligned}$$

$$\begin{aligned} BD &= 1 - F(x_m) \\ &= 1 - (2/aT)(1 - e^{-aT/2}) \qquad (14) \\ &= -20.77\% \\ x_o &= 0 \\ x_m - x_o &= 0.35x = 0.500aT \end{aligned}$$

True Triangle, $F(t_-) = (1 + t)$, $-1 \le t \le 0$

$F(t_+) = (1 - t)$, $0 \le t \le 1$

As with the cusp, $F(x_o) = 1$.

$$\begin{aligned} \text{For } T &= 0.7 \text{ (70\% of } t_{1/2} = 1) \\ a &= 1 \end{aligned}$$

$$\begin{aligned} BD &= 1 - F(x_m) \\ &= 1 - (1 - aT/4) = aT/4 \qquad (15) \\ &= 17.5\% \\ x_o &= 0 \\ x_m &= 0.3500 \\ x_m - x_o &= 0.3500 = 0.500aT \end{aligned}$$

Recapitulation. Normalization to $t_{1/2}$ is an aid to evaluating the sensitivity to ballistic deficit in the networks covered here. While $t_{1/2}$ is not the ideal normalization, it's better than t_p or $t_{.01}$. For pulse shapes exhibiting continuous derivatives at their peaks, *BD* is proportional to $(T/t_{1/2})^2$, and there is little difference in performance between the various networks. For the pulse shapes exhibiting discontinuous derivatives, the *BD* is linear with $T/t_{1/2}$ and is much worse than for pulse shapes with continuous derivatives. The sine^n and cusp filters are the best and worst performers; the true triangle is second worse.

L. Amplifier Noise

Noise has been extensively investigated [5], [8], [13-18]. It will be reviewed in this section, but to a large degree the orientation will be towards pulse-width normalization.

Symbols referring to noise quantities will be enclosed by carets. For example, $\langle v_p^2 \rangle$ and $\langle v_p \rangle$ refer to *ms* and *rms* step-noise voltages, respectively. The *ms* uncorrelated noise signals add as simple sums of their absolute values, but *rms* quantities add quadratically—as the square root of the sum of the squares. Most of the references here will be to *ms* rather than to *rms* values because that allows simple addition to be used in computing the total noise from the figures given in Table 2.

It has become the custom to use the term 'noise' when what is really meant is *NSR*, the ratio of *rms* noise to peak signal (or, to be consistent with the practice stated in the preceding paragraph, the square of that ratio). That custom will be continued here.

It should be recognized that the term 'noise figure' as used in the communications field (db above the minimum that can occur at the working temperature) is not used in the nuclear-electronics field because it doesn't lead to the kind of information that's useful, such as FWHM, *rms* equivalent electrons, etc.

Forms of Noise. The noise as it is affected by the width of the shaped pulse appears at the output of the amplifier in three forms: impulse or delta noise $\langle v_i^2 \rangle$, step noise $\langle v_p^2 \rangle$, and $1/f$ or flicker noise $\langle v_f^2 \rangle$. Resistors connected in series between the detector and preamplifier give rise to delta noise, as does the input FET. Resistors effectively in parallel with the signal source, such as the preamplifier feedback resistor and the detector bias resistor (in ac-coupled preamplifiers) give rise to step noise, as does thermally-generated detector current and FET gate current. Surface leakage currents and dielectric losses give rise to $1/f$ noise [17].

For a filter network, $\langle v_i^2 \rangle$ is inversely proportional to the width of the shaped pulse, $\langle v_p^2 \rangle$ directly proportional to it, and $\langle v_f^2 \rangle$ invariant with it. Because $\langle v_i^2 \rangle$ and $\langle v_p^2 \rangle$ are inversely related, a noise minimum occurs at the shaping index where the two components are equal. The $1/f$ component has no influence on where the minimum occurs, but does increase its level.

The effectiveness of a noise filter is characterized by its figure of merit $[\langle v_i^2 \rangle \langle v_p^2 \rangle]^{1/4}$. The cusp has the best possible one with a value of unity [2]; the *CR*-$(RC)^1$ network has the worst with a value of 1.359.

If amplifier noise limits the attainable energy resolution, and best possible resolution is the primary requirement, the system must be operated at a low counting rate and at a shaping index that minimizes the electronic noise.

When high-rate performance is required, the index must

be reduced to optimize the energy resolution (see Fig. 2), but at that optimum the resolution is never as good as the one at a lower rate. Since the product of impulse and step noise components is constant for a given network, reducing the shaping index causes impulse noise to dominate.

If ballistic deficit is a contributing factor, the resolution minimum will be shifted to a larger shaping index. Ordinarily, that does not occur with germanium detectors because $t_{1/2}$ at the noise minimum is much greater than the collection time in the detector.

Impulse and step noise are referred to sometimes as series and parallel noise respectively, but this terminology is misleading: it refers to the location in the circuit where the noise is generated rather than to its form. As a practical matter, the misleading terminology does not result in incorrect numbers: $\langle v_i^2 \rangle$ and $\langle v_p^2 \rangle$ begin as impulses having durations equal to the time it takes for an electronic imbalance—either in the detector or in one of the resistors—to appear at the input of the preamplifier. The frequency spectrum associated with the impulses is 'white', —the power density is invariant with frequency. If the impulses are integrated by a time constant large compared with $t_{1/2}$, they become approximations to steps, which is what happens at the input of low-noise preamplifiers where the resistors in parallel with that input are always large enough to meet the preceding condition. The resistors in series with the detector and preamplifier are always too small for that, and impulse noise remains as such.

Disregarding the equivalent noise generators and focusing on the effects of the filter-network transfer functions, the three forms are expressed in the following formulas:

$$\langle \zeta_i^2 \rangle = \frac{1}{2\tau}\langle \xi_i^2 \rangle = \frac{1}{2\pi\tau[F(t_o)]^2}\int_o^\infty \omega^2 |G(\omega)|^2 d\omega \quad (16)$$

$$= \frac{1}{2\tau[F(t_o)]^2}\int_o^\infty |F'(t)|^2 dt \quad (17)$$

$$\langle \zeta_p^2 \rangle = \frac{\tau}{2}\langle \xi_p^2 \rangle = \frac{\tau}{2\pi[F(t_o)]^2}\int_o^\infty |G(\omega)|^2 d\omega \quad (18)$$

$$= \frac{\tau}{2[F(t_o)]^2}\int_o^\infty |F(t)|^2 dt \quad (19)$$

$$\langle \zeta_f^2 \rangle = 4\langle \xi_f^2 \rangle = \frac{1}{[F(t_o)]^2}\int_o^\infty \omega |G(\omega)|^2 d\omega \quad (20)$$

Symbols in Eqs. 16-20. The symbols $\langle \zeta_i^2 \rangle$, $\langle \zeta_p^2 \rangle$, and $\langle \zeta_f^2 \rangle$ represent the influence of the shaping networks on the delta, step, and flicker noise components, respectively.

In Eq. 18 (step-noise), $|G(\omega)|^2$ represents the absolute value squared of the system transfer function in the frequency domain, including that portion due to the impedance at the interface between the detector and preamplifier. The term resulting from that impedance cancels the ω^2 term that appears in the delta-noise Eq. 16.

Eq. 19 is the same as Eq. 18, except for being in the time domain. Both domains require evaluation of integrals. With some waveforms the work is about the same whichever domain is chosen; with others, it may be easier to work in one than in the other.

Eqs. 16 and 17 for delta noise are the same as Eqs. 18 and 19, except that ω^2 in Eq. 16 manifests itself in Eq. 17 as $F'(t)$.

The time-domain equivalent of the flicker-noise Eq. 20 is not given because in this instance there is a clearcut advantage to working in the frequency domain.

$[F(t_o)]^2$ is the peak amplitude squared of the signal in the time domain and appears in each of the equations. It corresponds to the *S* in *NSR*.

In each of the equations, τ represents the network time constant (unity in Table 2). It is missing in the flicker-noise formulation, signifying that $1/f$ is invariant with shaping time. Note also that $[\langle \xi_i^2 \rangle \langle \xi_p^2 \rangle]^{1/4}$, the figure of merit, is invariant with τ; as the step-noise component increases with increasing shaping index, the delta-noise component decreases.

Fig. 12 and Table 2. The figure and the table contain nearly all of the quantitative data used in this report.

The organization of Fig. 12 is described in its caption. The bar lengths were obtained from Table 2.

The meanings of the rows and columns of Table 2 are given in its legend and caption.

The noise figures in the table were obtained by solving Eqs. 16 - 20, then multiplying by a constant to give unit values for the cusp in Rows C, D, and E. Those numerical constants (x0.5 or x4) are the multipliers on the $\langle \xi^2 \rangle$ terms in Eqs. 16 - 20; it is the $\langle \xi^2 \rangle$ terms that actually appear in Table 2. The remaining noise figures are then relative to those of the cusp. To compute the *NSR* for a particular filter network, the values listed in the table for the applicable shaper are used in conjunction with the equations. The total *ms* noise is the simple sum of the step, delta, and $1/f$ components. An example is given in App. A.

To be consistent with other parts of this report, the symbol x_y should have been used in the 1st column of Rows S, X, AA, and FF to indicate a normalization; the t_y signature is used instead because of the more familiar association of t with time.

The leading- and trailing-edge values in the table can be computed explicity only for the ideal waveforms; for the others, a root-finding routine must be used to solve the equation $[F(t)/F(t_o) - y] = 0$, where y is the fraction of peak pulse height for which the LE_y and TE_y values are desired.

Computations for the ballistic-deficit figures in the table were described earlier.

Normalization and the NSR. In support of the earlier work, $t_{1/2}$ proves to be the best choice for normalization.

In Fig. 12, the $t_{1/2}$ bars are the only ones to show a constant-amplitude step-noise index—approximately 0.75—for the Gaussian, quasi-Gaussian, and quasi-triangular waveforms, with only a small variation for the true-triangle and cusp. Also with $t_{1/2}$, the impulse noise shows an orderly progression downwards for the Gaussian and

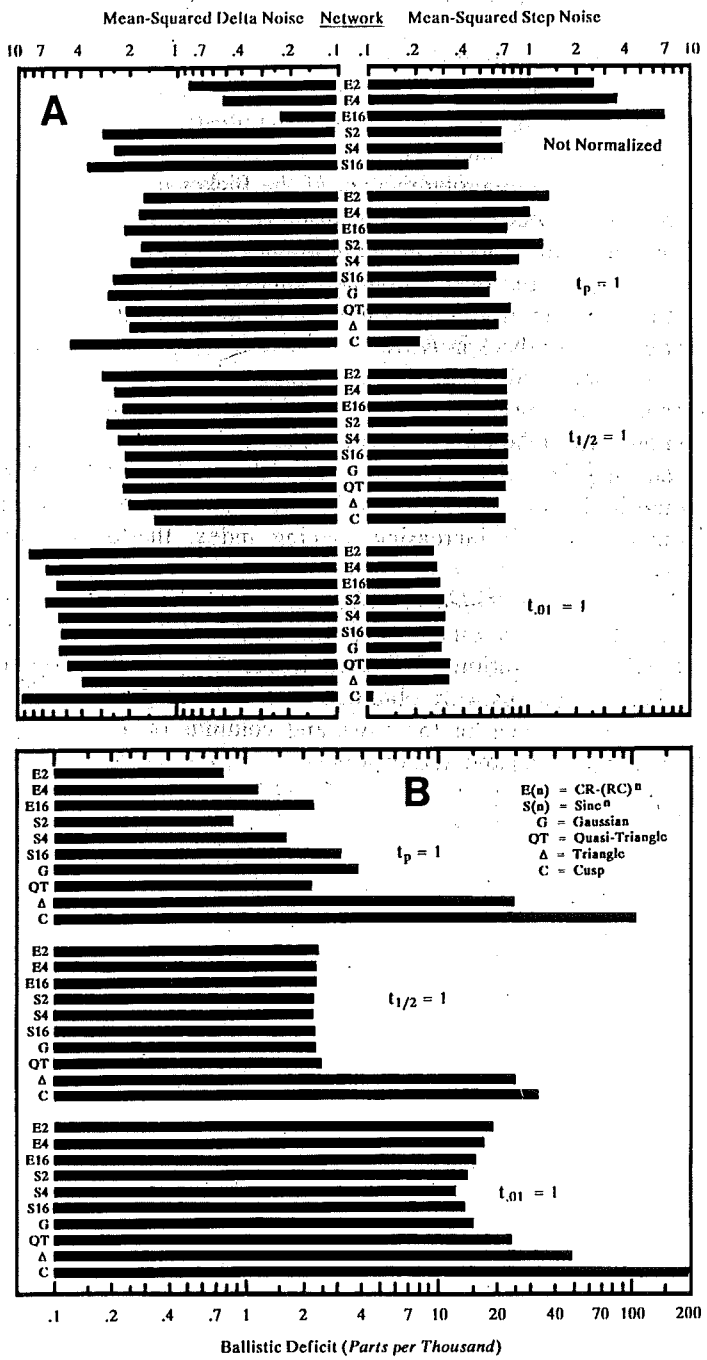

Fig. 12. (A) Step noise, impulse noise, and (B) ballistic deficit normalized to $t_p = 1$, $t_{1/2} = 1$, and $t_{.01} = 1$ for the networks listed in the legend at the upper right-hand corner of B.

In A, the bars extend to the right for ms step noise and to the left for ms impulse noise. Because of the logarithmic scale, the sum of the lengths for a given network is independent of the normalization.

In B, a 'step'-function driving signal having a linear rise is assumed, with the rise having a duration of 10% of the normalization time.

The bar lengths were obtained from Table 2. For example, the lengths of the bottom-most bars in A are 9.2103 for the impulse noise (Col. 2, Row GG in Table 2) and 0.1086 for the step noise (Col. 2, Row HH). In B, the length of the topmost bar is 0.7703 (Col. 7, Row V).

LEGEND for TABLE 2

Columns

Col. 1. Pulse-shaping parameters. These are defined in the lines where they first appear.

Cols. 2 - 4. 'Ideal' pulse shapes:

Cusp	$F(x) = e^{-\lvert x\rvert}$
True Gaussian	$F(x) = \exp(-x^2)$
True Triangle	$F(x) = (1 + x),\ -1 \le x \le 0$
	$= (1 - x),\ 0 \le x \le 1$

Col. 5. Quasi-triangular:
$F(x) = e^{-3x}(7.64 \sin^2 x + 2.53 \sin^4 x + 37.74 \sin^6 x)$.

Cols. 6-11. CR-(RC)^n: $F(x) = (x^n/n!)\, e^{-x}$, n = 1 - 16.

Cols. 12-16. Sine^n: $F(x) = e^{-3x} \sin^n x$, n = 2 - 16.

Rows

Row A. Pulse-shaping family.

Row B. Pulse shape (Cols. 2 - 4) and the number of low-pass sections n in the network (Cols. 6 - 16).

Row C. Numerical value, impulse-noise integral with a = 1:

$$\langle \epsilon_i^2 \rangle = a[F(t_o)]^{-2} \int_0^\infty |F'(t)|^2\, dt.$$ See text, Sec. L.

Row D. Numerical value, step-noise integral with a = 1:

$$\langle \epsilon_p^2 \rangle = (1/a)[F(t_o)]^{-2} \int_0^\infty |F(t)|^2\, dt.$$ See text, Sec. L.

Row E. Numerical value, flicker-noise integral divided by four (blanks were not evaluated):

$$\langle \epsilon_f^2 \rangle = 0.25[F(t_o)]^{-2} \int_0^\infty |G(\omega)/\omega|^2\, d\omega.$$ See text, Sec. L.

In evaluating the NSR, the numbers in Rows C and D must be halved, those in Row E multiplied by 4. The values in Row E apply also to the rows below S because the 1/f-noise integral is invariant with a.

Row F. Figure of merit (for noise) = $[\langle \epsilon_i^2 \rangle \langle \epsilon_p^2 \rangle]^{1/4}$.

Row G. Peak pulse height resulting from a unit-height step input. If the same non-inverting gain-of-1 amplifier stage is used to generate the sine^n and CR-(RC)^n filters (except for required differences in the ratios of the time constants), the $F(t_o)$'s in this row will also be the network transmission factors. For the sine^n filter, $F(t_o)$ increases with n while for the CR-(RC)^n network it decreases. For $n \ge 4$, the sine^n network exhibits substantially greater transmission efficiency than the CR-(RC)^n filter.

Rows H - L. Instant of time LE_y at which the Leading Edge of a pulse crosses the fraction y of the peak height.

Row M. Instant of time t_o at which a pulse peaks.

Rows N - R. Instant of time TE_y at which the Trailing Edge of a pulse crosses the fraction y of the peak height.

Rows H - R. Parameters before normalization, i.e., $a = 1/\tau = 1$.

Row S. Values of a for $t_p = 1$. Numerically, $a = (t_o - LE_{.01})$, where t_o is obtained from Row I, and $LE_{.01}$ is obtained from Row M.

Row T. Numbers in Row C divided by the a's from Row S.

Row U. Numbers in Row B multiplied by the a's of Row S. The figure of merit is not affected by the normalizations in Rows T - HH.

Row V. Ballistic Deficit (parts per thousand), unit-height 'step' with linear risetime T (0-100%) of 0.1 time units (10% of t_y).

Row W. Peak shift—due to ballistic deficit—from the original $at_o = x_o$ to the time $at_m = x_m$. Shift is exactly 0.5T for the ideal pulses and close to that for the actual ones.

Rows X - JJ. Repeats of Rows S - W for $t_{0.9}$, $t_{1/2}$, and $t_{.01}$; a for $t_{0.9} = TE_{0.9} - LE_{0.9}$ from Rows N and L, a for $t_{1/2} = TE_{0.5} - LE_{0.5}$ from Rows O and K, etc.

Row KK. Pulse-symmetry factors. Symmetry factor is exactly 1.0 for the ideal pulses, greater for all others.

Row LL. Pulse widths at 1% of peak height normalized to the width at 50%. This is a measure of resolving time.

Row MM. Same as Row LL, but for the width at 0.1%.

Table 2

This table contains the noise, ballistic deficit, and pulse-shaping parameters associated with the networks listed in Cols. 2-16. The waveforms correspond to F(x), where x=at. The parameter 'a' is a normalizing factor that forces the condition t_y=1, where t_y is the width of the pulse measured at the fraction 'y' of peak height.

All pulses in Rows S - MM have unit height except as affected by ballistic deficit. It follows that $F(t_o)=F(x_o)$, where the subscript 'o' stands for the time at which the peak of the pulse occurs.

The 1/f-noise components for the normalized pulses below Row S are the same as in Row E; 1/f noise is invariant with 'a'.

A complete legend for the columns and rows appears at the left.

A comparison of the pulse shapes of principal interest abstracted from the complete table and normalized to $t_{1/2}$=1 is shown in the mini-table at the right. Entries in each column have been further normalized to a lowest value of 1.0. Col. 2 shows the noise figure of merit (from Row F in the main table), Col.3 the relative resolving time at $t_{.001}$, Col. 4 the relative BD, and Col. 5 a figure of merit that indicates a tradeoff between noise and resolving time when the BD can be ignored, as is usually the case when $t_{1/2}$ is at or to the right of the noise minimum (see Fig. 2). It can be seen that with this criterion the best waveform is the true triangle, followed by the quasi-Δ and sine^6; the cusp is the worst.

1 Pulse Shape	2 Noise F. of M.	3 Resolving Time	4 Ballistic Deficit	5 Normalized Cols. 2 x 3
Cusp	1.000	4.988	15.11	4.642
Triangle	1.075	1.000	11.15	1.000
Quasi-Δ	1.132	1.258	1.100	1.325
Sine^6	1.135	1.387	1.000	1.466
Gaussian	1.120	1.580	1.029	1.646
CR-(RC)^6	1.148	1.672	1.042	1.786

	1	2	3	4	5	6	7	8	9	10	11	12	13	14	15	16	
A		IDEAL			QUASI TRI.	CR-(RC)^n						SINE^n					A
B	PARAMETERS	CUSP	GAUSS'N	TRI.		n = 1	2	4	6	8	n = 16	n = 2	4	6	8	n = 16	B
C	$a\langle\epsilon_i^2\rangle$	1.0000	1.2533	2.0000	2.1294	1.8473	0.8531	0.5117	0.3974	0.3360	0.2293	2.9977	2.4912	2.6075	2.8185	3.6954	C
D	$(1/a)\langle\epsilon_p^2\rangle$	1.0000	1.2533	0.6667	0.7716	1.8473	2.5593	3.5820	4.3719	5.0395	7.1083	0.6918	0.6975	0.6374	0.5792	0.4323	D
E	$\langle\epsilon_f^2\rangle$	1.0000	1.5708	1.3863		1.8473	1.7062	1.6375	1.6150	1.6039	1.5873	1.7081	1.6394				E
F	Fig. Merit	1.0000	1.1195	1.0746	1.1322	1.3591	1.2156	1.1636	1.1481	1.1405	1.1299	1.2000	1.1481	1.1354	1.1303	1.1242	F
G	$F(t_o)$	1.0000	1.0000	1.0000	1.0001	.36788	.27067	.19537	.16062	.13959	.09922	.34271	.34346	.37545	.41229	.54928	G
H	$LE_{.001}$	-6.9078	-2.6283	0.0010	.01164	.00037	.02354	.28070	.79719	1.4963	5.3350	.00734	.07515	.17876	.28236	.58105	H
I	$LE_{.01}$	-4.6052	-2.1460	.0100	.03832	.00369	.07644	.53146	1.2650	2.1709	6.7163	.02380	.14071	.27780	.39858	.70615	I
J	LE $LE_{.1}$	-2.3026	-1.5174	.1000	.14130	.03822	.26573	1.0855	2.1529	3.3581	8.8775	.08224	.28066	.45551	.58952	.88702	J
K	$LE_{.5}$	-.69315	-.83256	.5000	.48008	.23196	.76124	2.0828	3.5583	5.1149	11.741	.23204	.51751	.71348	.84563	1.1033	K
L	$LE_{.9}$	-.10536	-.32459	.9000	.81661	.60834	1.4191	3.1508	4.9447	6.7709	14.233	.42422	.75250	.94456	1.0632	1.2736	L
M	t_o	0	0	1	1.0144	1	2	4	6	8	16	.58800	.92795	1.1071	1.2120	1.3854	M
N	$TE_{.9}$	0.10536	0.32459	1.1000	1.2099	1.5318	2.7212	4.9896	7.1957	9.3695	17.907	.78408	1.1189	1.2791	1.3666	1.4989	N
O	$TE_{.5}$	.69315	.83256	1.5000	1.5183	2.6783	4.1559	6.8379	9.3635	11.807	21.826	1.1515	1.4454	1.5613	1.6158	1.6780	O
P	TE $TE_{.1}$	2.3026	1.5174	1.9000	1.9381	4.8897	6.7292	9.9462	12.891	15.693	26.129	1.7389	1.9128	1.9502	1.9541	1.9177	P
Q	$TE_{.01}$	4.6052	2.1460	1.9900	2.3214	7.6384	9.7794	13.458	16.773	19.892	31.385	2.3127	2.3308	2.2922	2.2511	2.1303	Q
R	$TE_{.001}$	6.9078	2.6283	1.9990	2.6218	10.233	12.587	16.600	20.188	23.543	35.788	2.7069	2.6135	2.5282	2.4596	2.2851	R
	Pulse parameters above this line are not time-normalized (LE: Leading Edge, TE: Trailing Edge, a = 1)																
S	t_p = 1, a	4.60517	2.14597	0.9900	.97612	.99631	1.9236	3.4685	4.7350	5.8921	9.2837	.56420	.78659	.82936	.81345	.67930	S
T	$a\langle\epsilon_i^2\rangle$	4.60517	2.68956	1.9800	2.0785	1.8404	1.6401	1.7750	1.8819	1.9795	2.1288	1.6913	1.9596	2.1626	2.2927	2.5103	T
U	$(1/a)\langle\epsilon_p^2\rangle$	0.21715	0.58403	.67340	.79045	1.8541	1.3305	1.0327	.92330	.85529	.76567	1.2261	.88679	.76854	.71196	.63637	U
V	BD*	-106.79	-3.8259	-24.75	-2.179	-.4134	-.7703	-1.252	-1.555	-1.805	-2.240	-.8615	-1.609	-2.146	-2.511	-3.176	V
W	$(x_m - x_o)$	0.05000	0.05000	0.0500	0.0499	0.0508	0.0508	0.0507	0.0507	0.0506	0.0505	0.0507	0.0505	0.0503	0.0503	0.0501	W
X	$t_{0.9}$ = 1,a	0.21072	0.64919	0.2000	.39331	.92347	1.3022	1.8389	2.2510	2.5986	3.6737	.35986	.36640	.33452	.30337	.22536	X
Y	BD*	-5.2496	-0.3511	5.0000	-.3545	-.3352	-.3531	-.3521	-.3518	-.3516	-.3513	-.3506	-.3495	-.3496	-.3498	-.3504	Y
Z	$(x_m - x_o)$	0.05000	0.05000	0.0500	0.0500	0.0508	0.0505	0.0504	0.0503	0.0503	0.0502	0.0505	0.0502	0.0502	0.0501	0.0500	Z
AA	$t_{1/2}$ = 1,a	1.38629	1.66511	1.0000	1.0383	2.4464	3.3947	4.7551	5.8052	6.6925	9.4420	.91951	.92784	.84777	.77017	.57464	AA
BB	$a\langle\epsilon_i^2\rangle$	1.38629	2.08690	2.0000	2.2109	4.5191	2.8960	2.4333	2.3072	2.2484	2.1650	2.7564	2.3115	2.2106	2.1708	2.1235	BB
CC	$(1/a)\langle\epsilon_p^2\rangle$	0.72135	0.75269	.66667	.74311	.75510	.75391	.75330	.75310	.75299	.75284	.75232	.75179	.75185	.75197	.75227	CC
DD	BD*	-33.870	-2.3066	-25.00	-2.465	-2.487	-2.395	-2.350	-2.335	-2.328	-2.317	-2.285	-2.240	-2.242	-2.251	-2.274	DD
EE	$(x_m - x_o)$	0.05000	0.05000	0.0500	0.0499	0.0520	0.0514	0.0510	0.0508	0.0507	0.0505	0.0511	0.0506	0.0504	0.0502	0.0501	EE
FF	$t_{.01}$ = 1,a	9.20134	4.29192	1.9800	2.2831	7.6347	9.7030	12.927	15.508	17.721	24.668	2.2889	2.1901	2.0145	1.8525	1.4242	FF
GG	$a\langle\epsilon_i^2\rangle$	9.21034	5.37912	3.9600	4.8615	14.103	8.2776	6.6150	6.1637	5.9537	5.6566	6.8613	5.4560	5.2528	5.2213	5.2628	GG
HH	$(1/a)\langle\epsilon_p^2\rangle$	0.10857	0.29202	.33670	.33795	.24196	.26376	.27710	.28190	.28437	.28815	.30223	.31850	.31641	.31263	.30354	HH
II	BD*	-198.63	-15.146	-49.50	-11.80	-23.65	-19.24	-17.12	-16.45	-16.11	-15.62	-14.01	-12.36	-12.55	-12.91	-13.83	II
JJ	$(x_m - x_o)$	0.05000	0.05000	0.0500	0.0499	0.0563	0.0540	0.0527	0.0522	0.0519	0.0513	0.0529	0.0514	0.0508	0.0506	0.0502	JJ
KK	$t_{.01}/2t_p$	1.00000	1.00000	1.0000	1.1695	3.8315	2.5222	1.8635	1.6376	1.5201	1.3286	2.0284	1.3922	1.2145	1.1387	1.0483	KK
LL	$t_{.01}/t_{1/2}$	6.64386	2.57757	1.9800	2.1989	3.1208	2.8583	2.7185	2.6715	2.6480	2.6127	2.4892	2.3604	2.3762	2.4053	2.4783	LL
MM	$t_{.001}/t_{1/2}$	9.96579	3.15686	1.9980	2.5139	4.1829	3.7009	3.4320	3.3402	3.2942	3.2253	2.9359	2.7358	2.7714	2.8269	2.9654	MM
	1	2	3	4	5	6	7	8	9	10	11	12	13	14	15	16	

*BD in parts per thousand, T = 0.1

quasi-Gaussian waveforms as the filter complexity increases, and is the only normalization for which the lengths of the bars give an accurate measure of the networks' figures of merit. (The proportionality is as the 1/4th root of those figures. Regarding delta-noise invariance, there is no pulse-width normalization that yields one.)

The variation in step noise for the quasi-Gaussian family (including the true Gaussian) is less than 0.5% for the $t_{1/2}$ normalization. If the normalization is made to $t_{.4715}$, the variation is reduced to 0.02% for the complete family (or to 0.001% if the sine^n group is excluded). However, the inconvenience of using that normalization does not compensate for the tighter invariance.

It would seem that the fraction 0.4715 should be simply related to a constant such as π or e, but no such relationship has been found.

Recapitulation. When the noise performance of the various shaping networks is compared, it is found that normalization to $t_{1/2}$ gives a more orderly progression than normalization to t_p or $t_{.01}$. With $t_{1/2}$, step noise is invariant throughout the quasi-Gaussian series, and impulse noise decreases monotonically as n increases for the CR-$(RC)^n$ and sine^n networks, with the latter giving lower noise for a given n than the former. By a small margin, the true-Gaussian waveform has the best figure of merit within the subgroup (but its resolving time is worse). That of the Q-T waveform is intermediate between the sine^6 and sine^8 shapes.

Through use of Table 2, the evaluation of noise integrals can be avoided. Waveforms not included in this report can be compared with those in Fig. 10, then an interpolation can be made from the figures in the table.

The difference in noise performance between waveforms is small. The difference in resolvings time is greater and can be obtained from Rows LL and MM in the table.

M. Normalization and Spectrometer Measurements.

The preceding information is used now to explain the differences between the resolution curves in Figs 2-4, beginning with Fig. 2 (normalization to $t_{1/2}$). Before analyzing the data, the following comments are necessary:

The amplifiers available for the tests did not yield enough data points for adequate curve fitting. Those that were available were connected by smooth curves as shown, but a later test on a single amplifier better suited to the purpose revealed that at short shaping times, the trace is a straight line that abruptly changes into the characteristic parabolic shape. The straight region is dominated by ballistic deficit, the parabolic region by noise.

The preceding situation adversely affects the correlation between theory and practice in the following descriptions.

Normalization to $t_{1/2}$. Resolution at the left-hand end of the curves should be controlled mainly by *BD*. From Row DD in Table 2, *BD* = 2.47 x 10^{-3} for the Q-T filter vs 2.24 x 10^{-3} for the sine^n. This is borne out by the curves. The separation between the 2 kCPS and 62 kCPS curves is greater than it should be for the reason given in the opening paragraphs of this section.

At the right hand end of the 2kCPS curves, resolution is controlled mainly by step noise. Except for small differences in the performance of the main amplifiers, the curves should have merged, and they nearly do. At 62 kCPS, resolution is controlled by pile-up and the performance of the *BLR*'s. The curves should follow the resolving-time progression shown in Row LL of Table 2, $t_{.01}/t_{1/2}$. The Q-T and sine^6 curves do, but the sine^4 curve does not. A possible explanation is that the *BLR* in the sine^n amplifier is inferior to the ones used in the others.

Normalization to t_p. From Row V, Table 2, the *BD* for the sine^4 filter is 1.60 x 10^{-3}, vs 2.18 x 10^{-3} for the Q-T filter. This difference is borne out by the curves at the left-hand end of the figure.

At the right-hand end of the 62 kCPS curves, the resolution follows the resolving-time progression shown in Row KK of Table 2.

At the right-hand end of the 2 kCPS curves, the resolution of the sine^4 amplifier is greater than that of the sine^6 or Q-T amplifiers, confirmed by the step-noise figures in Row U of Table 2.

Normalization to $t_{.01}$. At the left-hand end of the curves, the sine^4 amplifier shows substantially worse resolution than the others, much more than can be explained by the numbers in Row II of Table 2. The most likely reason is that this amplifier had additional filtering to reduce output noise at the shorter shaping times, a practice not uncommon among amplifier manufacturers. The effect on pulse shape is to broaden it at the 1% level. When the pulse is normalized at $t_{.01}$, the width near the peak is narrower than it should be for the expected transfer function, increasing the apparent *BD* and worsening the resolution. The skewing is not apparent for $t_{1/2}$ or t_p.

The 62 kCPS curves should have merged at the right-hand end because all exhibit the same resolving time when normalized to $t_{.01}$. The fact of the resolution difference between the sine^4 and the other amplifiers implies that the *BLR* in the sine^4 unit does not match the performance of the others.

From Row HH of Table 2, the step noise is worst for the Q-T network, successively improving for the sine^4 and sine^6 filters. At the right-hand end of the 2 kCPS curves, the Q-T and sine^6 amplifiers follow the progression, but the sine^4 unit is better than it should be. This ties in with the preceding comments about additional filtering: the spreading at $t_{.01}$ would compress the width at $t_{1/2}$, reducing the apparent step noise.

Recapitulation. At $t_{1/2}$, two systems can be compared for their resolution capabilities at high and low counting rates and at short, intermediate, and long shaping times. At $t_{.01}$, the effect of ballistic deficit at the shorter shaping times is emphasized. At t_p, performance differences at high count rates and long shaping times are magnified.

It appears that by comparing resolution measurements between two systems normalized at $t_{1/2}$, t_p, and $t_{.01}$, information can be obtained about their relative performance not readily accessible by other means. For

the user, this is an evaluation tool—for the designer, a diagnostic tool.

N. Generalizations: the Effect of Pulse Shape on Noise

It was stated earlier that the noise index of a filter does not depend on the transfer function per se, but on the shape of the waveform as displayed on an oscilloscope.

Because of their geometric and mathematical simplicity, the unit-height triangle and unit-height trapezoid, (Figs. 13 and 14) are used to lay the groundwork for the rules to follow. Begin with the triangle in Fig. 13.

Triangle. With a baseline two units wide, $t_{1/2} = 1$.

For the leading edge: $F_1(t) = t/t_o$; for the trailing edge: $F_2(t) = (2 - t)/(2 - t/t_o)$. In what follows, the subscripts 1 and 2 will be used to identify operations on the two parts of the pulse. Later, computations on the trapezoid will require three subscripts.

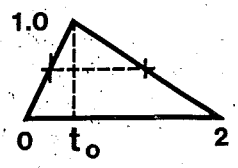

Fig. 13. Triangular pulse.

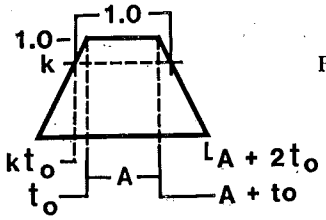

Fig. 14. Trapezoidal pulse

Noise computations consist of evaluating Eqs. 17 and 19. Consideration will be limited to $\langle \xi^2 \rangle$ so that a direct comparison may be made with the entries in Table 2.

In place of the original 0 and ∞ for the limits on the $\langle \xi^2 \rangle$ integral, the limits become 0 and t_o for $\langle \xi^2 \rangle_1$; for $\langle \xi^2 \rangle_2$, they become t_o and $(2 - t_o)$. The changes reflect the fact that unlike the exponential waveforms that have trailing edges of infinite duration, those of the two parts of the triangle are finite.

The evaluation of Eq. 19 (*ms* step noise) leads to $\langle \xi_p^2 \rangle_1 = \langle \xi_p^2 \rangle_2 = 1/3$. The two components sum to 2/3 as shown in Col. 4, Row D in Table 2. Evidently, the *ms* step noise depends only on the width of the baseline and is independent of the lateral position of t_o above it.

The evaluation of Eq. 17 (*ms* delta noise) leads to $\langle \xi_i^2 \rangle_1 = 1/t_o$, and $\langle \xi_i^2 \rangle_2 = 1/(2 - t_o)$. Their sum is $2/[t_o(2 - t_o)]$. The two parts are different. If $t_o = 1$, $\langle \xi_i^2 \rangle_1 = \langle \xi_i^2 \rangle_2$, making $\langle \xi_i^2 \rangle_1 + \langle \xi_i^2 \rangle_2 = 2$, in accordance with Col. 4, Row C in Table 2. The pulse symmetry resulting from setting $t_o = 1$ also results in a minimum-noise condition for a triangle. This does not prove that symmetry always leads to minimum noise, but examination of the quasi-Gaussian and true-Gaussian entries in Table 2 shows the same pattern. This should come as no surprise, because *ms* delta noise depends on the quadratic sum of the derivatives of the two halves of the waveforms: the squaring action magnifies differences in slope, with the larger portion disproportionately dominating the sum. The sum is minimized when the slopes of the halves are equal, and the equality is concomitant with symmetry between the leading and trailing halves of the shaped pulse.

Trapezoid. Having established that asymmetry worsens impulse noise, only the symmetrical trapezoid of Fig. 14 will be considered.

The figure has three regions: the first from 0 to t_o, the second from t_o to $(A + t_o)$, and the last from $(A + t_o)$ to $(A + 2t_o)$. Those regions fix the limits of integration in Eqs. 17 and 19.

From the analysis of the triangle, the *ms* delta noise for the first and last regions sums to $\langle \xi_i^2 \rangle = 2/t_o$. In the central region, $F'(t_o) = 0$; that region contributes nothing to the delta noise.

The step noise associated with the first and last regions is $2t_o/3$. In the central region, $F_2(t) = 1$, $\langle \xi_p^2 \rangle_2 = A$, and the total step noise is $\langle \xi_p^2 \rangle = A + 2t_o/3$.

Now consider what happens when the ramps pivot about their point of intersection with level k.

In the case of the quasi-Gaussian waveform, the step noise was invariant with $t_{1/2}$, hinting that a similar condition applies to the trapezoid. To find out, set the pulse width at level k equal to unity: $[A + 2t_o(1 - k)] = 1$. By transposing, $A = [1 + 2t_o(k - 1)]$. From the second paragraph above, $\langle \xi_p^2 \rangle = (A + 2t_o/3)$. Replacing A with $[1 + 2t_o(k - 1)]$, then setting $d\langle \xi_p \rangle/dk = 0$, we find that $k = 2/3$, or $t_{2/3} = 1$ for the step noise to be invariant with the width between the pivot points.

With the preceding condition, it follows that the step noise of the trapezoid under consideration is 1.00, which is 1/3rd greater than for the triangle with $t_{1/2} = 1$. This is in accordance with the increase in the baseline, which went from 2 to 8/3.

If the ramp slopes are unchanged from the triangle in which $t_{1/2} = 1$, the impulse noise also will be unchanged.

It seems that there is no advantage to a trapezoid over a triangle because noise and resolving time are worse. However, the *BD* is reduced: it can be shown that $BD = 0$ if $T \leq A$. In the example just given, $T = A = 1/3$ if $t_o = 1$. In Table 2, a duration of $T = 0.1$ was assumed. By reducing A from 1/3 to 0.1 without changing the slope of the ramps, the baseline is shrunk, improving the resolving time, keeping $BD = 0$, and reducing the step noise without affecting the delta noise.

At this point, it should be appreciated that by thinking in terms of a normalized pulse width, it becomes relatively easy to examine the tradeoffs between noise, resolving time, and *BD*.

Examination of the triangle and trapezoid is now complete. Flicker noise is next.

Flicker Noise. It can be shown that evaluation of $\langle \xi_f^2 \rangle$ leads to *ms* noise which is proportional to the logarithm of (f_h/f_l) [5], where f_h and f_l are the high- and low-frequency cutoff points of the filter. The 1/*f* noise is invariant with t_y because the ratio f_h/f_l is fixed for a given network, regard-

less of t_y. But $f_h/f_l = |F'(t_y)|/t_y = [\langle \xi_i^2 \rangle \langle \xi_p^2 \rangle]$. The last term is the kernel of the figure of merit, and it follows that $1/f$ noise should be invariant with it. From the figures in Table 2 and over the span of the quasi-Gaussian and true-Gaussian family, the fractional change in *ms* flicker noise compared with that of the figure of merit is <3.5%.

For a given $t_{1/2}$, the $1/f$ noise should follow the trend of delta noise. It does, but the dependence is weak. For example, the ratio of $\langle \xi_i^2 \rangle$ of the CR-$(RC)^2$ network to that of the true Gaussian (Row BB) is 1.39, while the ratio of $\langle \xi_f^2 \rangle$ for the same combination (Row E) is only 1.09.

Ratio of Pulse Height to Pulse Width. In Fig. 5, imagine tangents to the sides of the waveform extended up to their point of intersection. From the preceding discussions, those tangents will produce a triangle with approximately the same step and impulse noise as the original waveform, but with a greater peak height. It follows that such a pulse shape will have a better *SNR* than the original for no other reason than that the S is greater, as is borne out by the figures of merit for the applicable waveforms in Table 2.

Recapitulation. For a given $t_{1/2}$, pulse symmetry minimizes impulse noise. Also, with a symmetrical pulse, the *ms* noise varies directly with the slope of one of the edges, therefore inversely as the width of the pulse. For asymmetrical pulses, the steeper of the leading- or trailing-edge slopes will dominate the noise dependency.

The *ms* step noise varies directly with the width of the shaped pulse. For the quasi-Gaussian and true-Gaussian family, the step noise is nearly invariant with $t_{1/2}$.

The *ms* flicker noise is a weak function of pulse shape, being proportional to the log of the ratio of risetime to width, and is invariant with $t_{1/2}$.

For a symmetrical trapezoid, step noise is invariant with $t_{2/3}$.

Appendix A, Use of Table 2 in Computing Noise

In this example of computing the *ms* input noise charge in a preamplifier, only the delta and step noise components are considered. Eqs. 16 and 18 will be used. The appropriate noise sources and the noise indices from Table 2 must be included. The example will be for a sine^6 network, normalized to $t_{1/2}$, and with a shaping index of 2.5μs. The figures from the table are at Col. 14, Rows BB (2.211) and CC (0.752). Those figures are for τ = 1 sec. The modified equations are as follows:

$$\langle q_i^2 \rangle = 4kT_\epsilon R_s C_\epsilon^2 \frac{1}{2\tau} \langle \xi_i^2 \rangle \qquad (21)$$

$$\langle q_p^2 \rangle = \left[\frac{4kT_\epsilon}{R_p} + 2e_o I \right] \frac{\tau}{2} \langle \xi_p^2 \rangle \qquad (22)$$

The first noise generator (impulse noise, Eq. 21) is represented by $4kT_\epsilon R_s$, where k is Boltzman's constant, T_ϵ is temperature, and R_s is the resistance that appears in series with the detector and the input of the preamplifier. In a semiconductor detector the contacts and the undepleted material contribute to that resistance. Also included is the equivalent noise resistance of the input transistor. In a modern FET, this is $\approx 0.9/G_M$, with G_M in units of A/V). The resistance from all sources is assumed to total 100Ω.

A temperature of 289K (17 °C) is assumed, making $4kT_\epsilon = 1.60 \times 10^{-20}$.

The quantity C_ϵ represents the noise-equivalent input capacitance of the system ('cold' input capacitance in farads. See App. B), including that due to the detector, preamplifier, and connecting wires.

There are two step-noise generators (Eq. 21). The first is associated with R_p, the parallel combination of all resistors shunting the input of the preamplifier to ground. Those were described in Sec. L. The second is associated with thermally-generated current 'seen' by the preamplifier. The quantity e_o represents the electronic charge.

The parameters assumed for this example are as follows:

$$\begin{aligned} k &= 1.38 \times 10^{-23} \text{J/K} \\ T_\epsilon &= 289\text{K (17 °C)} \\ 4kT_\epsilon &= 1.6 \times 10^{-20} \\ R_s &= 100\Omega \\ R_p &= 2.5 \times 10^{9}\Omega \\ C_\epsilon &= 100 \times 10^{-12}\text{F} \\ I &= 1 \times 10^{-9}\text{A} \\ e_o &= 1.6 \times 10^{-19}\text{C} \\ \tau &= 2.5 \times 10^{-6}\text{s} \\ \langle \xi_i^2 \rangle &= 2.211 \\ \langle \xi_p^2 \rangle &= 0.752 \end{aligned}$$

When inserted into the equations, the following results are obtained:

$$\begin{aligned} \langle q_i^2 \rangle &= 70.5 \times 10^{-34} \textit{ ms} \text{ Coulombs} \\ \langle q_i \rangle &= 8.40 \times 10^{-17} \textit{ rms} \text{ Coulombs} \end{aligned}$$

$$\begin{aligned} \langle q_p^2 \rangle &= (0.006 + 3.01) \times 10^{-34} \textit{ ms} \text{ Coulombs} \\ \langle q_p \rangle &= 1.75 \times 10^{-17} \textit{ rms} \text{ Coulombs} \end{aligned}$$

It can be seen that the noise due to R_p (the 1st component of $\langle q_p^2 \rangle$) is negligible compared with that due to the leakage current (2nd component). By equating the two it can be shown that the crossover occurs when the noise current flowing through the resistor produces a dc-voltage drop of 50mV [5].

The agreement between measurement and computation in determining $\langle q_i \rangle$ is usually about 5%, but the agreement for $\langle q_p \rangle$ is not as good, particularly at large shaping indexes, partly because of the indeterminacy of dielectric losses seen by the input, and partly because distributed capacitance to ground at the high-megohm feedback resistor (if used) appears as $1/f$ noise [17] not easily distinguished from step noise.

To convert $\langle q_n \rangle$ to eV FWHM (Ge), $\langle q_n \rangle$ first must be divided by e_o to obtain *rms* equivalent electrons, then multiplied by ϵ = 2.95 eV per electron to obtain eV *rms* for a germanium detector, and finally multiplied by 2.35 to

convert from *rms* to FWHM.

App. B, Cold Input Capacitance

The noise-equivalent input capacitance of a preamplifier is that which is measured with the signal path broken, but with all dc operating voltages applied to the transistors. That condition is difficult to impose, and an alternative must be used.

The procedure* is to prepare a group of low-noise capacitors in shielded containers that can be plugged into the input of the preamplifier, then to plot a curve of shaping-amplifier output noise vs external input capacitance (values from 0 to 100pF in a binary series are appropriate). The meter used to measure output noise must be true-rms or average-indicating with a bandwidth of at least 10 MHz, the capacitance values must be known with an error of less than 1%, losses in pulse height that may result at the higher capacitances must be corrected for, and the measurement must be made at the shortest possible shaping index so that delta noise controls. The 'curve' will be a straight line which, when extrapolated, will intersect the abscissa at a value of $-C$. The absolute value of that C represents the noise-equivalent input capacitance.

If the step noise is not negligible, that fact will manifest itself as concave-upwards curvature of the lower part of the line. If that occurs, only the straight portion should be used to make the extrapolation.

In principle, only two (large) external capacitors are needed for the test, C_1 and C_2, with $C_2 \approx 2C_1$. When plugged into the preamplifier, the total capacitance will be $(C_1 + C_c)$ and $(C_2 + C_c)$. With two measurements, two points on the line will be established, from which the slope and zero intercept can be determined. However, with just two points, there is no assurance that the line is straight.

Acknowledgements

The writer gratefully acknowledges the help received in various ways from A. M. Ferrari of the Nuclear Engineering Sciences Department, University of Florida and from B. W. Coyne, T. R. Crawford, J. M. Dudley, and S. H. Hinshaw of Tennelec. Also, Tennelec furnished working space, test instruments, and materials which were necessary to carry out the work described in this report.

References

[1] *IEEE Standard Test Procedures for Amplifiers and Preamplifiers used with Detectors of Ionizing Radiation*, IEEE Standard 301-1988, IEEE, New York.

[2] H. den Hartog and F. A. Muller, "Optimum Instrument Response for Discrimination against Spontaneous Fluctuations", *Physica*, vol. 13 No. 9, pp. 571-580, Nov. 1947.

[3] C. H. Mosher, "Pseudo-Gaussian Functions with Superlative Baseline Recovery", *IEEE Trans. on Nucl. Sci.*, vol. NS-23, no. 1, pp. 226-228, Feb. 1976.

[4] F. S. Goulding, D. A. Landis and N. W. Madden, "Design Philosophy for High-Resolution Rate and Throughput Spectroscopy Systems", *IEEE Trans. Nucl. Sci.*, vol. NS-30 no. 1, pp. 301-310, Feb. 1983.

[5] A. B. Gillespie, *Signal, Noise and Resolution in Nuclear Counter Amplifiers*, McGraw-Hill Book Co., New York, NY, 1953.

[6] L. B. Robinson, "Reduction of Baseline Shift in Pulse Amplitude Measurements, *Rev. Sci. Instr.*, vol. 32, No. 9, p. 1057, Sept. 1961.

[7] E. Fairstein, "Gated Baseline Restorer with Adjustable Asymmetry", *IEEE Trans. Nucl. Sci.*, vol. NS-22, no. 1, pp. 463-466, Feb. 1975.

[8] E. Baldinger and W. Franzen, *Advances in Electronics and Electron Physics*, L. Morton, Editor, pp. 255-268, Academic Press, New York, 1956.

[9] B. W. Loo, F. S. Goulding, and D. Gao, "Ballistic Deficits in Pulse Shaping Amplifiers", *IEEE Trans. Nucl. Sci.*, vol. NS-35 no. 1, pp. 114-118, Feb. 1988.

[10] F. S. Goulding and D. A. Landis, "Ballistic Deficit Correction in Semiconductor Spectrometers", *IEEE Trans. Nucl. Sci.*, vol. NS-35 no. 1, pp. 119-124, Feb. 1988.

[11] T. W. Raudoff, M. O. Bedwell and T. J. Paulus, "Pulse Shape and Risetime Distribution Calculations for HPGe Coaxial Detectors", *IEEE Trans. Nucl. Sci.*, vol. NS-29 no. 1, pp. 764-768, Feb. 1982.

[12] D. K. Cheng, *Analysis of Linear Systems*, Addison-Wesley, Reading, Mass., 1959.

[13] N. R. Campbell, "The Study of Discontinuous Phenomena", Proc. Camb. Phil. Soc., vol. 15, pp. 117-136, 1908.

[14] S. O. Rice, "Mathematical Analysis of Random Noise, *Bell System Technical Journal*, vol. 23, pp. 282-333, 1944.

[15] R. Wilson, "Noise in Ionization Chamber Pulse Amplifiers", *Phil. Mag.*, vol. 41, pp. 66-76, Jan. 1950.

[16] M. S. Gupta, Editor, *Electrical Noise: Fundamentals & Sources**, IEEE Press, 1977, New York.

[17] V. Radeka, "State of the Art of Low Noise Amplifiers for Semiconductor Radiation Detectors", *Proc. International Symposium on Nucl. Elect., Versaille, 1968*, Sec. 46, pp. 1-28.

[18] F. S. Goulding, "Pulse Shaping in Nuclear Amplifiers: A Physical Approach to Noise Analysis", *Nucl.Instr. and Methods*, Vol. 100, pp. 493-504, 1972.

*This method is an outgrowth of Radeka's way of unbundling the various noise components [17].

*This is an excellent source book, containing many reprints and an extensive bibliography.